KA-TP-17-2008

Center-vortex loops with one selfintersection

Julian Moosmann and Ralf Hofmann

Institut für Theoretische Physik
Universität Karlsruhe (TH)
Kaiserstr. 12
76131 Karlsruhe, Germany

Abstract

We investigate the 2D behavior of one-fold selfintersecting, topologically stabilized center-vortex loops in the confining phase of an SU(2) Yang-Mills theory. This coarse-graining is described by curve-shrinking evolution of center-vortex loops immersed in a flat 2D plane driving the renormalization-group flow of an effective 'action'. We observe that the system evolves into a highly ordered state at finite noise level, and we speculate that this feature is connected with 2D planar high T_c superconductivity in $FeAs$ systems.

1 Introduction

The idea of a nontrivial ground state being responsible for the emergence of 'elementary' particles is a rather old one: Already Lord Kelvin proposed that atoms and molecules should be considered knotted lines of vortices representing distortions in a universal medium (or ground state) – the ether [1]. As we know now, the physics of atoms and molecules is described in terms of a much more efficient and elegant framework: Quantum mechanics. The agent responsible for the chemical bond – Kelvin's electron – is considered a spinning point particle in quantum mechanics, and this yields an excellent description of atomic physics, collider physics, and for the bulk of situations in condensed matter physics.

There are, however, theoretical discrepancies with the concept of the electron being a point particle, and there are exceptional experimental situations pointing to the limitations of this concept to describe reality. As for the former, we have the old problem of a diverging classical selfenergy not resolved in quantum electrodynamics where the electron mass is introduced as a free parameter whose running with resolution needs an experimental boundary condition. On the other hand, the two-dimensional dynamics of strongly correlated electrons in condensed matter physics signals the relevance of nonlocal effects possibly related to the nontrivial anatomy of the electron becoming relevant in collective phenomena [2, 3]. Also, recent high-temperature plasma experiments indicate unexpected explosive behavior not unlikely related to the mechanism for lepton emergence, see [4] and references therein.

Recent developments in understanding the confining phase of an SU(2) Yang-Mills theory suggest that Kelvin's ideas may actually be realized in Nature, see also [5]. The authors of [5] construct a plausible effective low-energy action for the 4D SU(2) Yang-Mills theory with solutions to the associated field equations representing closed confining strings knotted into stable solitons. In the thermodynamic approach of [6] the emergence of magnetic center-vortex loops (CVLs) is related to discontinuous phase changes of a complex order parameter for confinement across the (downward) Hagedorn transition and the fact that no magnetic charges exist where these flux lines could end. Also, it was discussed in [6] how the locations of topologically stabilized selfintersection represent isolated, spinning magnetic charges [1].

In our previous article [7] we have investigated the sector with $N = 0$ selfintersections by considering a resolution dependent ensemble average. The corresponding weight-functional is defined purely in terms of the planar curves's geometry. The resolution dependence of this geometry, in turn, is determined by a curve-shrinking equation (heat-equation) [8, 9]. The validity of this description of spatial coarse-graining is motivated from considerations relating local curvature with the direction and speed of 'motion' of the associated line-segment. The requirement that

[1] Notice that with respect to the electromagnetic U(1) of the Standard Model there is a dual interpretation of magnetic charges emerging in an SU(2) Yang-Mills theory.

the partition function over a given ensemble of planar curves is invariant under a change of the resolution then yields the renormalization-group evolution of the weight-functional which is written as the exponential of an 'action'. Here the term 'action' is slightly misleading since we do not aim at describing the time-evolution of the system by demanding stationarity of the 'action' under curve variation. To do the latter, a model, which relates resolution and time (being a macroscopic concept associated with the measuring apparatus), needs to be introduced. We thus regard resolution over time as the more fundamental quantity to describe certain subatomic systems. Our observation is that the effective 'action' exhibits a transition towards dilational invariance after a finite, critical decrease of resolution. On average, CVLs with $N = 0$ are shrunk to circular points for a resolution less than the critical value which defacto removes them from the spectrum and thus generates an asymptotic mass gap[2]. Knowing the evolution of the weight-functional, one is in a position to compute the resolution dependence of 'observables' as ensemble averages of the associated (nonlocal or local) 'operators'. As for the evolution of the initially sharp center-of-mass position, we observe a spread of the variance with decreasing resolution saturating at a finite value. This is similar to the unitary free-particle evolution of a position eigenstate in quantum mechanics.

The purpose of the present article is to extend the procedure of [7] to the case of $N = 1$. We now have a singled-out point on the curve: the location of the selfintersection where practically the entire mass of the soliton resides [6]. Setting the Yang-Mills scale Λ of the SU(2) theory equal to the electron mass $m_e = 511\,\mathrm{keV}$, which in turn determines the mass of the intersection point, we interprete this soliton as an electron or a positron [4, 10]. In the presence of a static electric or magnetic background field it is physically possible to lift the two-fold degeneracy w.r.t. the two possible directions of center-flux: The soliton exhibits a two-fold spin degeneracy. Notice that as long as both wings of center flux are of finite size the position of the intersection point can be shifted at almost no cost of energy. In particular, if the inner angle α between in- and out-going center-flux at the intersection is sufficiently small then a motion of points on the vortex line directed perpendicular to the bisecting line of the angle α easily generates a velocity of the intersection point which exceeds the speed of light, see Fig. 1. Recall, that the path-integral formulation of quantum mechanics admits such superluminal motion in the sense that the according trajectories sizably contribute to transition amplitudes.

The paper is organized as follows. In Sec. 2 we discuss the physics associated with the emergence of topologically stabilized CVLs with intersection number $N = 1$, and how their spatial 2D coarse-graining is captured by a curve-shrinking flow. Some mathematical results on the properties of this flow for immersed curves, which are relevant for our subsequent numerical analysis, are briefly discussed. Also, we repeat our discussion in [7] of how the renormalization-group flow of an effective 'action' is driven by the curve-shrinking evolution of the members of a given ensemble of

[2]CVLs with $N > 0$ are massive [6, 10].

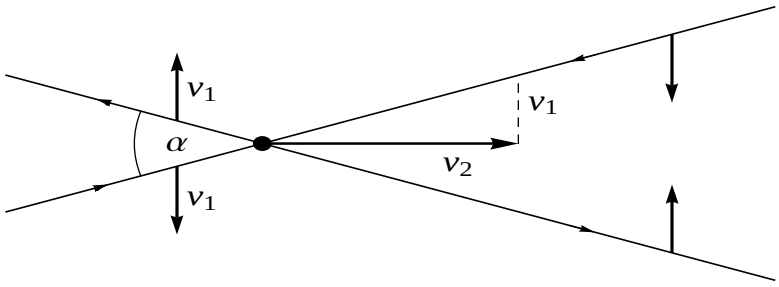

Figure 1: Points on the center flux lines moving oppositely on a line perpendicular to the bisecting line of the angle α with velocity modulus v_1. For sufficiently small α the velocity modulus v_2 of the intersection point is superluminal: $v_2 = v_1 \cot \frac{\alpha}{2}$.

curves. In Sec. 3 we explain our numerical analysis concerning the computation of the effective 'action', the variance of the location of the selfintersection, and the entropy associated with a given ensemble. Finally, in Sec. 4 we summarize our results and interprete them in view of certain 2D layered, quasimetallic systems exhibiting high-T_c superconductivity.

2 Conceptual framework

2.1 Selfintersecting center-vortex loops

The transition from the non-selfintersecting to the selfintersecting CVL sector is by twisting of non-selfinteresecting curves. The emergence of a localized (anti)monopole in the process is due to its capture by oppositely directed center fluxes in the intersection core (eye of the storm). By a rotation of the left half-plane in Fig. 2(a) by an angle of π, see Fig. 2(b), each wing of the CVLs forms a closed flux loop by itself thereby introducing equally directed center fluxes at the intersection point. This does not allow for an isolation of a single, spinning (anti)monopole in the core of the intersection and thus is topologically equivalent to the untwisted case Fig. 2(a). However, another rotation of the left-most half-plane in Fig. 2(c) introduces an intermediate loop which by shrinking is capable of isolating a spinning (anti)monopole due to oppositely directed center fluxes. Notice that in the last stage of such a shrinking process (short distances between the cores of the flux lines), where propagating dual gauge modes are available[3], there is repulsion due to Biot-Savart which needs to be overcome. This necessitates an investment of energy manifesting itself in terms of the mass of the isolated (anti)monopole (eye of the storm). Alternatively, the emergence of an isolated (anti)monopole is possible by a simple pinching of the untwisted curve, again having to overcome local repulsion in the final stage of this process.

For the analysis performed in the present work we solely regard the situation

[3]On large distances these modes are infinitely massive which is characteristic of the confining phase.

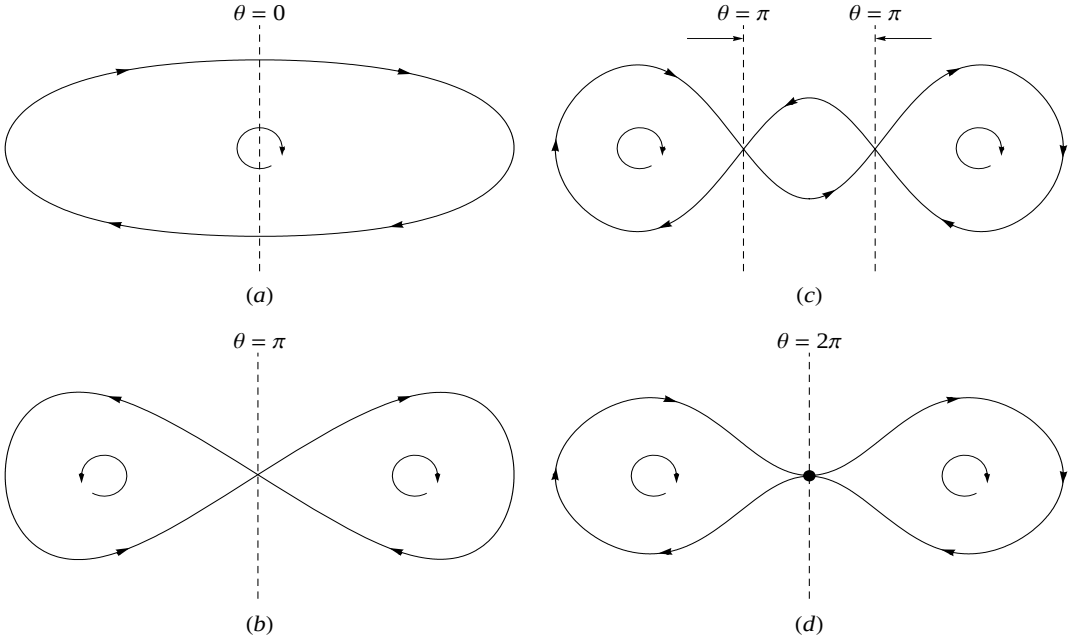

Figure 2: (Topological) transition from the $N = 0$ sector (a), (b), (c) to the $N = 1$ sector (d) by twisting and subsequent capture of a magnetic (anti)monopole in the core of the final intersection. Arrows indicate the direction of center flux.

depicted in Fig. 2(d) and thus no longer need to discuss the direction of center flux within a given curve segment: This is not relevant for the process of a spatial coarse-graining microscopically described by the same curve-shrinking flow as applied to sector with $N = 0$ [7].

2.2 Euclidean curve shrinking flow

Notice that by immersing an SU(2) CVL with finite core size d and mass m_d of the dual gauge field into a flat 2D surface at $m_D < \infty$, $d > 0$, a hypothetic observer measuring a positive (negative) curvature of a segment of the vortex line experiences more (less) negative pressure in the intermediate vicinity of this curve segment leading to its motion towards (away from) the observer, see Fig. 3. The (inward directed) speed of a point in the core of the vortex will be a monotonic function of the curvature at this point. On average, this shrinks the CVL. Alternatively, one may *globally* consider the limit $m_D \to \infty$, $d \to 0$, that is, the confining phase of an SU(2) Yang-Mills theory, but now take into account the effects of an environment which *locally* relaxes this limit (by collisions) and thus also induces curve shrinking. This situation is described by the following equation for a flow in the (dimensionless) parameter τ

$$\partial_\tau \mathbf{x} = \frac{1}{\sigma}\, \partial_s^2 \mathbf{x}\,, \tag{1}$$

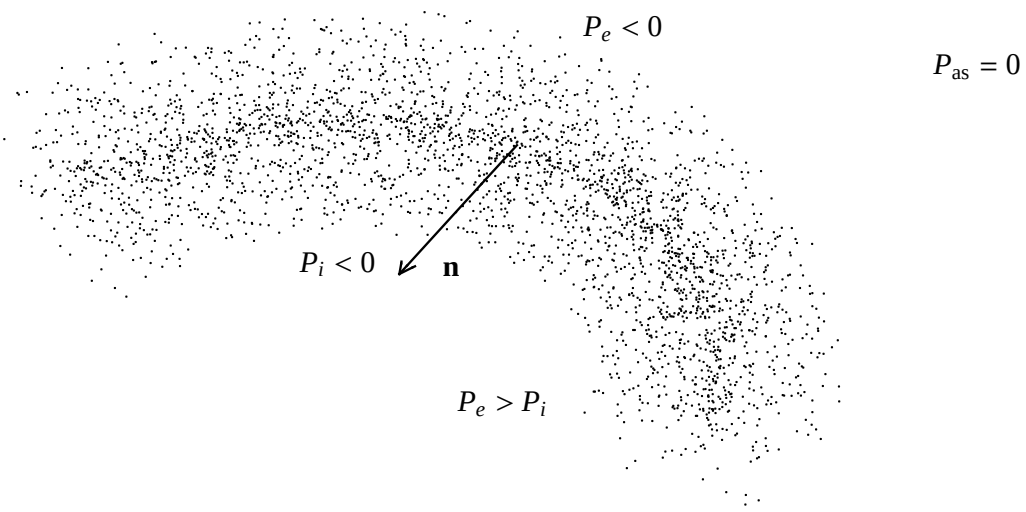

Figure 3: Highly space-resolved snapshot of a CVL segment. The pressure P_i in the region pointed to by the normal vector $\mathbf{n}$ is more negative than the pressure P_e thus leading to a motion of the segment along $\mathbf{n}$.

where s is arc length, $\mathbf{x}$ is a point on the CVL in the plane, and σ is a string tension effectively expressing the distortions induced by the environment. After a rescaling, $\hat{x} \equiv \sqrt{\sigma}\mathbf{x}$, $\xi = \sqrt{\sigma}s$, Eq. (1) assumes the following form

$$\partial_\tau \hat{x}(u,\tau) = \partial_\xi^2 \hat{x} = k(u,\tau)\mathbf{n}(u,\tau)\,, \tag{2}$$

where u is a (dimensionless) curve parameter, $\mathbf{n}$ the (inward-pointing) Euclidean unit normal, k the scalar curvature, defined as

$$k \equiv \left|\partial_\xi^2 \hat{x}\right| = \left|\frac{1}{|\partial_u \hat{x}|}\partial_u\left(\frac{1}{|\partial_u \hat{x}|}\partial_u \hat{x}\right)\right|\,, \tag{3}$$

$|\mathbf{v}| \equiv \sqrt{\mathbf{v}\cdot\mathbf{v}}$, and $\mathbf{v}\cdot\mathbf{w}$ denotes the Euclidean scalar product of the vectors $\mathbf{v}$ and $\mathbf{w}$. In the following we resort to a slight abuse of notation by using the same symbol $\hat{x}$ for the functional dependence on u or ξ.

We now consider curves with one selfintersection, that is $N = 1$, in the sense of the stable situation of Fig. 2(d). This situation was mathematically analysed in [12]. Since the direction of center flux is inessential for the shrinking process we may actually treat this situation in a way as depicted in Fig. 2(b), where the curve is defined to be a smooth immersion into the plane with exactly one double point and a total rotation number zero, $\int_0^L k\, d\xi = 0$. Here the (dimensionless) curve length L is given by the smooth integration $L(\tau) = \int_0^{L(\tau)} d\xi = \int_0^{2\pi} du\, |\partial_u \hat{x}(u,\tau)|$. Notice that this is topologically distinct from the case Fig. 2(d) where one encounters a nonvanishing rotation number which is not smoothly deformable to zero.

In the $N = 0$ case a smooth, embedded curve shrinks to a circular point under the flow for $\tau \nearrow T < \infty$ [8, 9]. That is, the isoperimetric ratio approaches 4π from

above. The curve in situation Fig. 2(b) separates the plane into three disjoint areas two of which are finite and denoted by A_1 and A_2. We understand by T the finite, critical value of τ where either A_1 or A_2 or both vanish. This corresponds to a singularity encountered and thus terminates the flow.

Recall that in the $N = 0$ case the rate of area change is a constant, $\frac{dA}{d\tau} = -2\pi$. This is no longer true for $N = 1$. However, we have that

$$A_1(\tau) - A_2(\tau) = \text{const}\,. \tag{4}$$

Also, for $N = 1$ we have in comparison to the $N = 0$ case the more relaxed constraint that $-4\pi \leq \frac{d(A_1+A_2)}{d\tau} \leq -2\pi$.

In contrast to the $N = 0$ case the isoperimetric ratio for the $N = 1$ case is bounded for $\tau \nearrow T$ if and only if $A_1 \neq A_2$. Notice that the case $A_1 = A_2$ physically is extremely fine-tuned.

2.3 Effective 'action'

We now wish to interprete curve-shrinking as a Wilsonian renormalization-group flow taking place in the $N = 1$ CVL sector in the sense defined in Sec. 2.2. A partition function, defined as a statistical average (according to a suitably defined weight) over $N = 1$ CVLs, is to be left invariant under a decrease of the resolution determined by the flow parameter τ. Notice that, physically, τ is interpreted as a strictly monotonic decreasing (dimensionless) function of a ratio $\frac{Q}{Q_0}$ where Q (Q_0) are mass scales associated with an actual (initial) resolution applied to the system. The role of Q can also be played by the finite temperature of a reservoir coupled to the system.

To device a geometric ansatz for the effective 'action' $S = S[\hat{x}(\tau)]$, which is a functional of the curve $\hat{x}$ representable in terms of integrals over local densities in ξ (reparametrization invariance), the following reflection on symmetries is in order. (i) scaling symmetry $\hat{x} \to \lambda\hat{x}\,, \quad \lambda \in \mathbf{R}_+$: For $\lambda \to \infty$, implying $\lambda L \to \infty$ at fixed L, the 'action' S should be invariant under further finite rescalings (decoupling of the fixed length scales $\sigma^{-1/2}$ and Λ^{-1}), (ii) Euclidean point symmetry of the plane (rotations, translations and reflections about a given axis): Sufficient but not necessary for this is a representation of S in terms of integrals over scalar densities w.r.t. these symmetries. That is, the 'action' density should be expressible as a series involving products of Euclidean scalar products of $\frac{\partial^n}{\partial\xi^n}\hat{x}\,, \quad n \in \mathbf{N}_+$, or constancy. However, an exceptional scalar integral over a nonscalar density can be deviced. Consider the area A, calculated as

$$A = \left| \frac{1}{2} \int_0^{2\pi} d\xi\, \hat{x} \cdot \mathbf{n} \right| . \tag{5}$$

The density $\hat{x} \cdot \mathbf{n}$ in Eq. (5) is not a scalar under translations.

We now resort to a factorization ansatz as

$$S = F_c \times F_{nc}\,, \tag{6}$$

where in addition to Euclidean point symmetry F_c (F_{nc}) is (is not) invariant under $\hat{x} \to \lambda\hat{x}$. In principle, infinitely many operators can be defined to contribute to F_c. Since the evolution homogenizes the curvature except for a small vicinity of the intersection point higher derivatives of k w.r.t. ξ should not be of importance. We expect this to be true also for Euclidean scalar products involving higher derivatives $\frac{\partial^n}{\partial\xi^n}\hat{x}$. To yield conformally invariant expressions such integrals need to be multiplied by powers of $\sqrt{A}$ and/or L or the inverse of integrals involving lower derivatives. At this stage, we are not capable of constraining the expansion in derivatives by additional physical or mathematical arguments. To be pragmatic, we simply set F_c equal to the isoperimetric ratio:

$$F_c(\tau) \equiv \frac{L(\tau)^2}{A(\tau)}\,. \tag{7}$$

We conceive the nonconformal factor F_{nc} in S as a formal Taylor expansion in inverse powers of L or $A \equiv A_1 + A_2$ due to the property of conformal invariance for $L, A \to \infty$.

Since we regard the renormalization-group evolution of the effective 'action' as induced by the flow of an ensemble of curves, where the evolution of each member is dictated by Eq. (2), we allow for an explicit τ dependence of the coefficient c of the lowest nontrivial power $\frac{1}{L}$ or $1/A$. In principle, this sums up the contribution to F_{nc} of certain higher-power operators which do not exhibit an explicit τ dependence. Hence we make the following ansatz

$$F_{nc}(\tau) = 1 + \frac{c(\tau)}{L(\tau)}\,. \tag{8}$$

The initial value $c(\tau = 0)$ is determined from a physical boundary condition such as the mean length $\bar{L}$ at $\tau = 0$.

2.4 Geometric partition function

Let us now numerically investigate the effective 'action' $S[\hat{x}(\tau)]$ resulting from a partition function Z w.r.t. a nontrivial ensemble E. The latter is defined as the average

$$Z = \sum_i \exp\left(-S[\hat{x}_i(\tau)]\right) \tag{9}$$

over the ensemble $E = \{\hat{x}_1, \cdots\}$. Let us denote by E_M an ensemble consisting of M curves where E_M is obtained from E_{M-1} by adding a new curve $\hat{x}_M(u, \tau)$. The effective 'action' S in Eq. (6) (when associated with the ensemble E_M we will denote it by S_M) is determined by the function $c_M(\tau)$, compare with Eq. (8), whose flow follows from the requirement of τ-independence of Z_M:

$$\frac{d}{d\tau} Z_M = 0\,. \tag{10}$$

This is an implicit, first-order ordinary differential equation for $c(\tau)$ which needs to be supplemented with an initial condition $c_{0,M} = c_M(\tau = 0)$. A natural initial condition is to demand that the quantity

$$\bar{L}_M(\tau = 0) \equiv \frac{1}{Z_M(\tau = 0)} \sum_{i=1}^{M} L[\hat{x}_i(\tau = 0)] \exp\left(-S_M[\hat{x}_i(\tau = 0)]\right) \tag{11}$$

coincides with the geometric mean $\tilde{L}_M(\tau = 0)$ defined as

$$\tilde{L}_M(\tau = 0) \equiv \frac{1}{M} \sum_{i=1}^{M} L[\hat{x}_i(\tau = 0)] \,. \tag{12}$$

From $\bar{L}_M(\tau = 0) = \tilde{L}_M(\tau = 0)$ a value for $c_{0,M}$ follows. We also have considered a modified factor

$$F_{nc}(\tau) = 1 + \frac{c(\tau)}{A(\tau)} \,. \tag{13}$$

in Eq. (6). While the ansatz for the geometric effective 'action' thus is profoundly different for such a modification of $F_{nc}(\tau)$ physical results such as the evolution of the variance of the intersection agree remarkably well, see Sec. 3.

3 Results of simulation

3.1 Preparation of ensembles

Similar as in [7] we normalize all curves to have the same initial area $A_0 = A_{0,1} + A_{0,2}$ and, since we are now interested in the position of the intersection where the (anti)monopole is localized, we have applied a translation to each curves in the ensembles E_M such that the location of the intersections initially coincide with the origin.

Since the critical value T of the flow parameter τ varies from curve to curve we order the members of the maximal-size ensemble $E_{M=16}$ into subensembles $E_{M<16}$ such that $T_{i=1} \geq T_{i=2} \geq \cdots \geq T_M$. The types of ensembles E_M obtained in this way are referred to as T-ordered. We also have performed all simulations with ensembles $E'_{M<16}$ whose members are picked randomly from $E_{M=16}$ and have obtained strikingly similar results for ensemble averages of 'observables' using $E_{M<16}$ and $E'_{M<16}$ for the τ evolution to the left of $\tau = \min\{T_i | \hat{x}_i \in E'_{M<16}\}$.

The maximal-size ensemble $E_{M=16}$ at $\tau = 0$ is depicted in Fig. 4 with the universal choice $A_0 = 200\,\pi$. The curves in Fig. 4 are arranged in a T-ordered way. We have $T_{i=1} = 65 \geq T_{i=2} \geq \cdots \geq T_M = 43$. In Fig. 5 the evolution of an initial curve under curve shrinking is shown from two view points. The flow is started at $\tau = 0$ and stopped at a value of τ shortly below T. In Fig. 6 the flow of the intersection points, corresponding to the initial curves depicted in Fig. 4, is shown. The

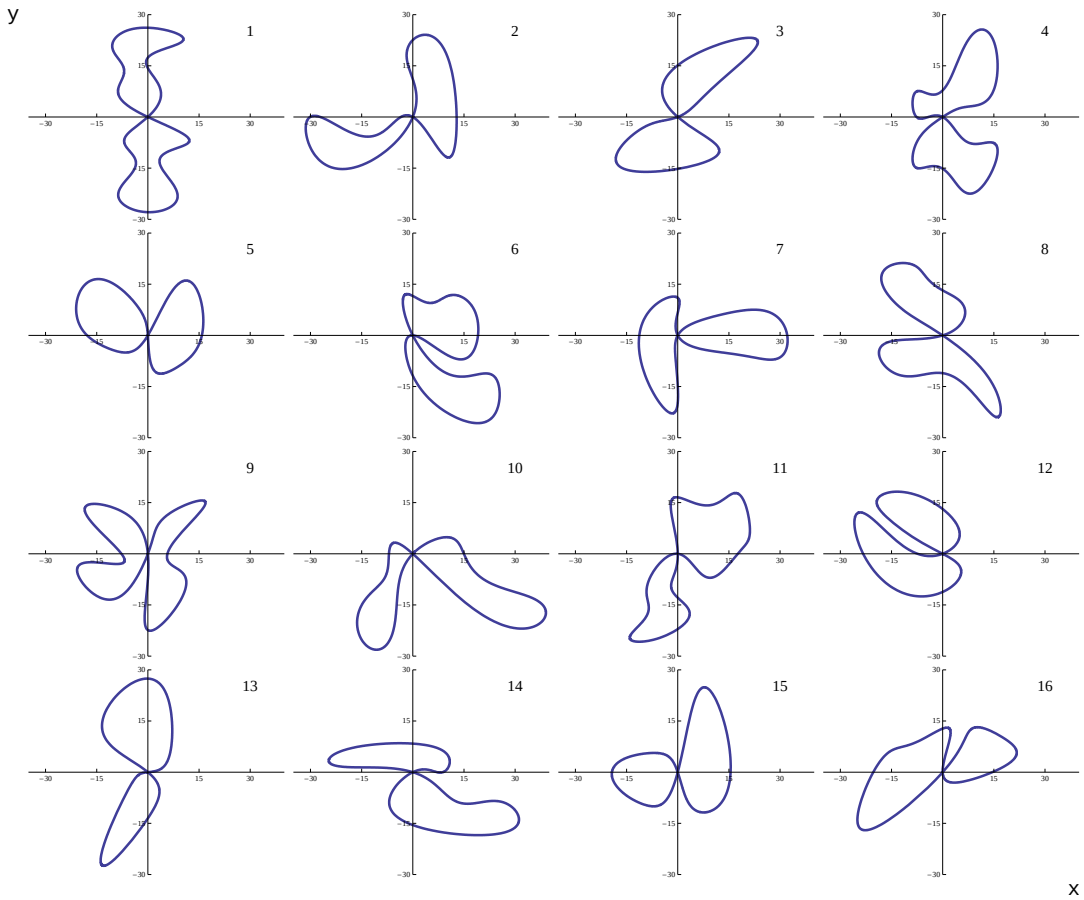

Figure 4: Initial curves $\hat{x}_i(u, \tau = 0)$ contributing to the ensemble $E_{M=16}$. The intersection points coincide with the origin, and all curves have the same area $200\,\pi$. By definition $E_{M=16}$ is T-ordered.

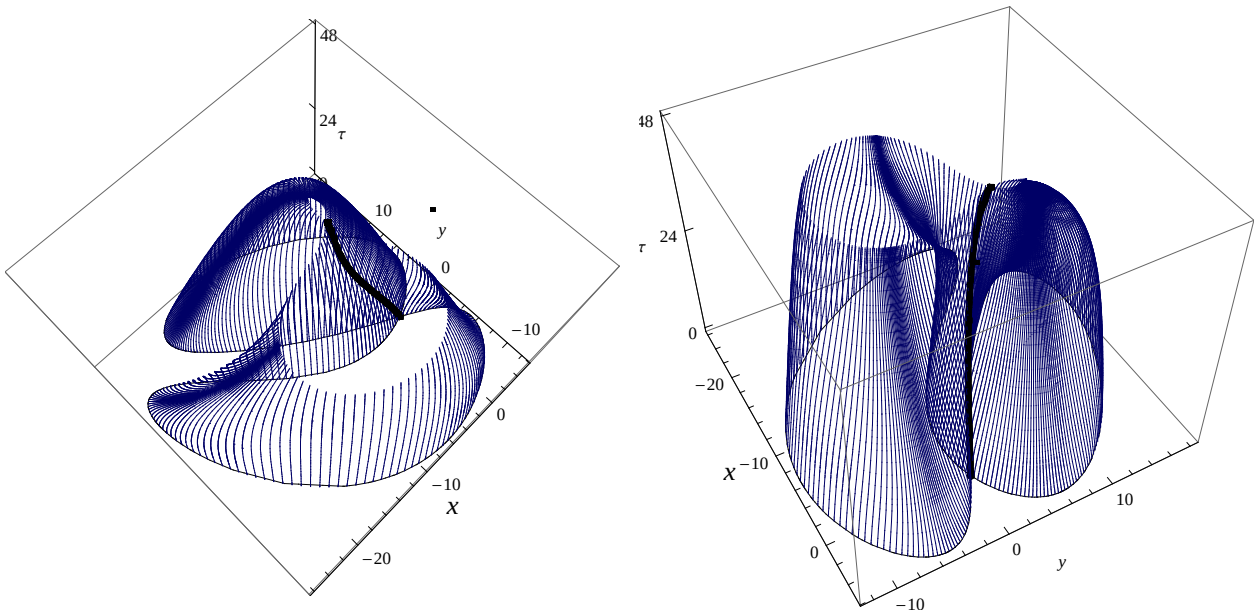

Figure 5: Plot of the evolution of an $N = 1$ CVL (curve 12 of Fig. 4) under Eq. (2). The thick central line indicates the trajectory of the intersection point which coincides with the origin at $\tau = 0$.

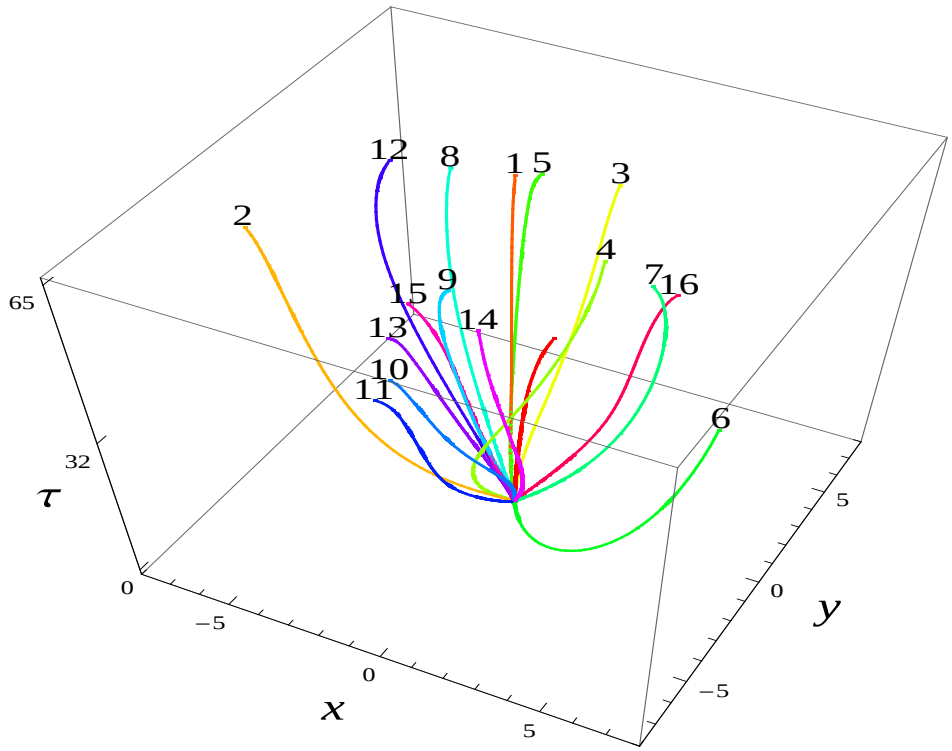

Figure 6: Flow of the intersection points for the initial curves depicted in Fig. 4.

search for solutions to the second-order PDE Eq. (2) subject to periodic boundary conditions in the curve parameter, $\hat{x}(u = 0, \tau = 0) = \hat{x}(u = 2\pi, \tau = 0)$, and for the initial conditions $\hat{x}(u, \tau = 0)$ depicted in Fig. 4 was performed numerically using the method of lines. That is, the PDE was discretized on a uniform grid in the parameter u yielding a semi-discrete problem in terms of a system of ODEs in τ which was solved using Mathematica. Fig. 5 indicates why this technique is called the numerical method of lines. As one can also see from Fig. 5, a set of discrete points on the curve, although remaining equidistant in u, may evolve under the flow such that the spatial distances between next-neighbours-points falls below the numerical precision. Numerically, the flow then encounters a singularity (not to confused with the earlier mentioned nonfictitious singularities). To recognize such a situation automatically, Eq. (4) was exploited: The evolution was stopped as soon as a sizable deviation occured from what Eq. (4) predicts. The configuration obtained at this point in τ was fitted in such a way that a new discretization in u yielded well separated points to re-start the methods of lines. Eq. (4) was also used as an indicator for the final singularity at T where A_1 or A_2 or both vanish.

3.2 Renormalization-group invariance of partition function

For all ensembles E_M the τ dependence of the coefficient c_M in Eq. (8) roughly behaves like a square root $\propto \sqrt{T_M - \tau}$ where T_M is the weakly ensemble-dependent minimal resolution. For the modified 'action' $S_M = \frac{L(t)^2}{A(t)} \left(1 + \frac{c_M(t)}{A(t)}\right)$ the coefficient c_M is well approximated by a linear function $\propto T_M - \tau$. Again, T_M denotes a weakly ensemble-dependent minimal resolution. For T-ordered ensembles the results for c_M for the 'actions' Eq. (8) and Eq. (13) are shown in Figs. 7 and 8, respectively. The

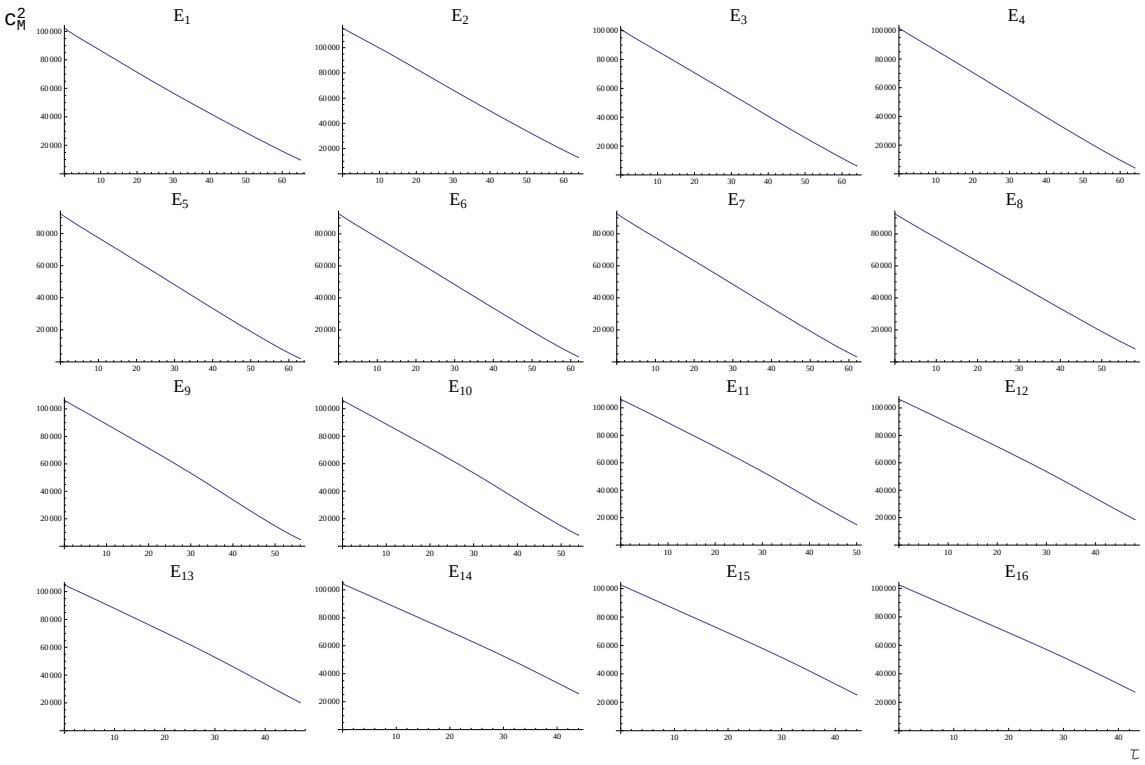

Figure 7: The squares of the coefficients $c_M(\tau)$ entering the ansatz for effective 'action' of Eq. (6) specializing to Eq. (8) for T-ordered ensembles up to $M = 16$.

results for ensembles E'_M do not differ sizably from those presented in Figs. (7), (8).

3.3 Variance of location of selfintersection

The mean intersection $\bar{\hat{x}}_{\rm int}$ over the ensemble E_M is defined as

$$\bar{\hat{x}}_{\rm int}(\tau) \equiv \frac{1}{Z_M} \sum_{i=1}^{M} \hat{x}_{{\rm int},i}(\tau) \exp\left(-S_M[\hat{x}_i(\tau)]\right) \,, \tag{14}$$

where $\hat{x}_{{\rm int},i}(\tau)$ is the location of selfintersection (intersection point) of curve $\hat{x}_i$ at τ. The scalar statistical deviation $\Delta_{M,{\rm int}}$ of $\bar{\hat{x}}_{\rm int}$ over the ensemble E_M is defined as

$$\Delta_{M,{\rm int}}(\tau) \equiv \sqrt{{\rm var}_{M,{\rm int};x}(\tau) + {\rm var}_{M,{\rm int};y}(\tau)} \,, \tag{15}$$

where

$$\begin{aligned} {\rm var}_{M,{\rm int};x} &\equiv \frac{1}{Z_M} \sum_{i=1}^{M} \left(x_{{\rm int},i}(\tau) - \bar{x}_{\rm int}(\tau)\right)^2 \exp\left(-S_M[\hat{x}_i(\tau)]\right) \\ &= -\bar{x}^2_{\rm int}(\tau) + \frac{1}{Z_M} \sum_{i=1}^{M} x^2_{{\rm int},i}(\tau) \exp\left(-S_M[\hat{x}_i(\tau)]\right) \end{aligned} \tag{16}$$

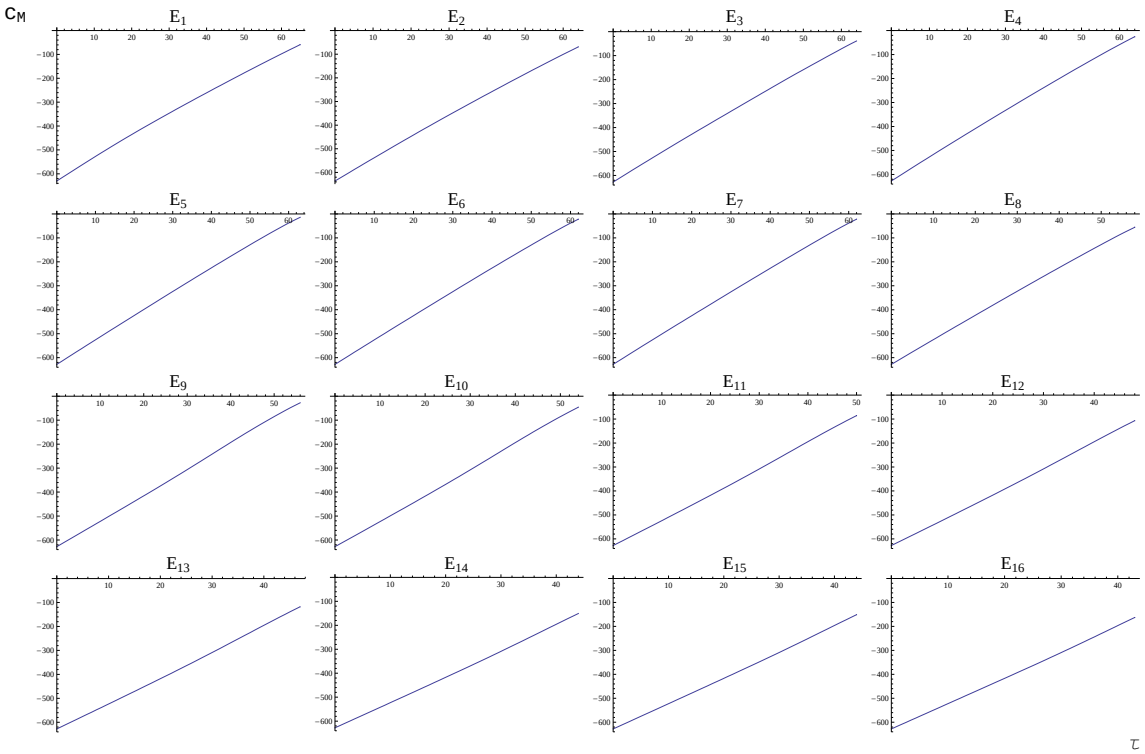

Figure 8: The coefficient $c_M(\tau)$ entering the ansatz for the effective 'action' of Eq. (6) specializing to Eq. (13) for T-ordered ensembles up to $M = 16$.

and similarly for the coordinate y. In Fig. 9 plots of $\Delta_{M,\mathrm{int}}(\tau)$ are shown when evaluated over the ensembles $E_1, \cdots, E_{16}$ subject to the 'action'

$$S_M = \frac{L(\tau)^2}{A(\tau)} \left(1 + \frac{c_M(\tau)}{L(\tau)}\right)$$

and the initial condition $\bar{L}_M(\tau = 0) = \tilde{L}_M(\tau = 0)$. In Fig. 10 the according plots of $\Delta_{M,\mathrm{int}}(\tau)$ are depicted as obtained with the 'action'

$$S_M = \frac{L(\tau)^2}{A(\tau)} \left(1 + \frac{c_M(\tau)}{A(\tau)}\right)$$

and subject to the initial condition $\bar{L}_M(\tau = 0) = \tilde{L}_M(\tau = 0)$. Relaxing the constraint of T-ordering ($E_M \to E'_M$) does not entail a qualitative change of the results.

The results presented in Figs. 9, 10 are unexpected since in the $N = 0$ sector the variance of the 'center-of-mass' saturates rapidly to finite values. In contrast, for the $N = 1$ sector the variance of the location of selfintersection initially increases, reaches a maximum, and decreases to zero at a *finite* value of τ. This is readily confirmed by the evaluation of the entropy, see Sec. 3.4.

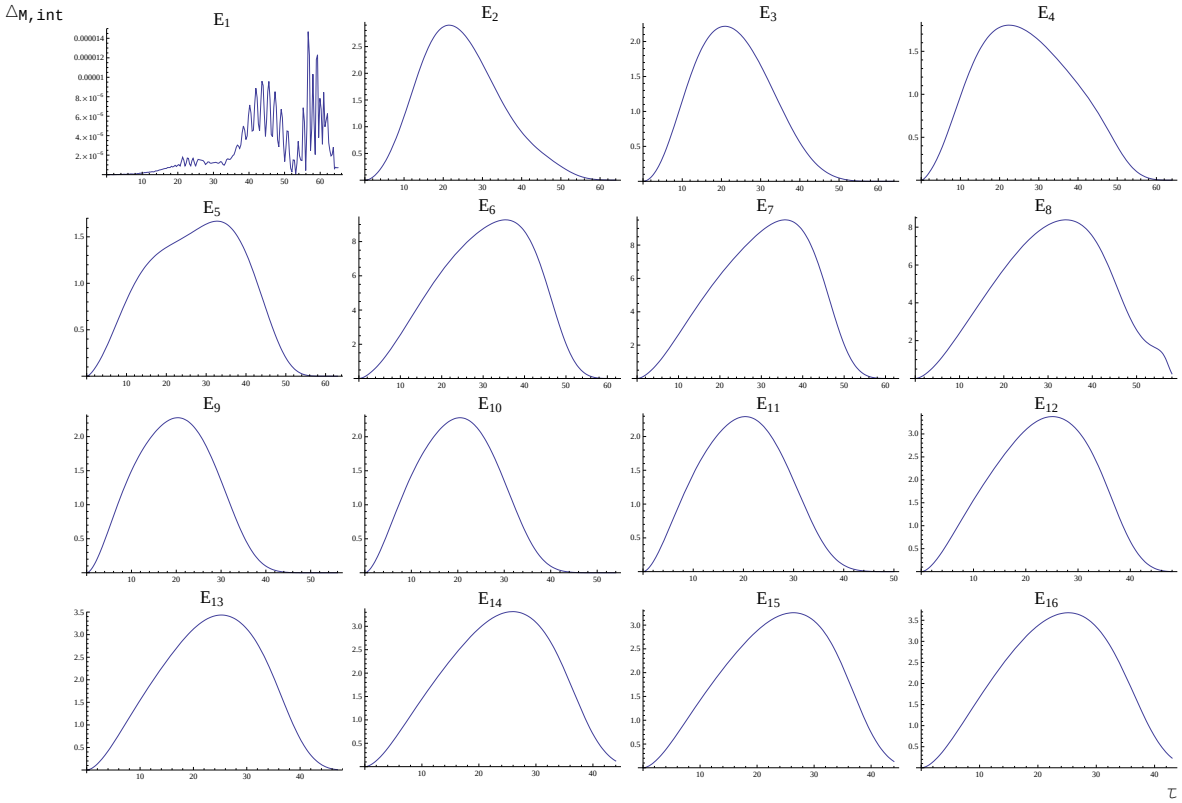

Figure 9: Plots of $\Delta_{M,\mathrm{int}}(\tau)$ for the T-ordered ensembles E_M with $M = 1, \cdots, 16$. We have employed the ansatz for the 'action' $S_M = \frac{L(\tau)^2}{A(\tau)}\left(1 + \frac{c_M(\tau)}{L(\tau)}\right)$.

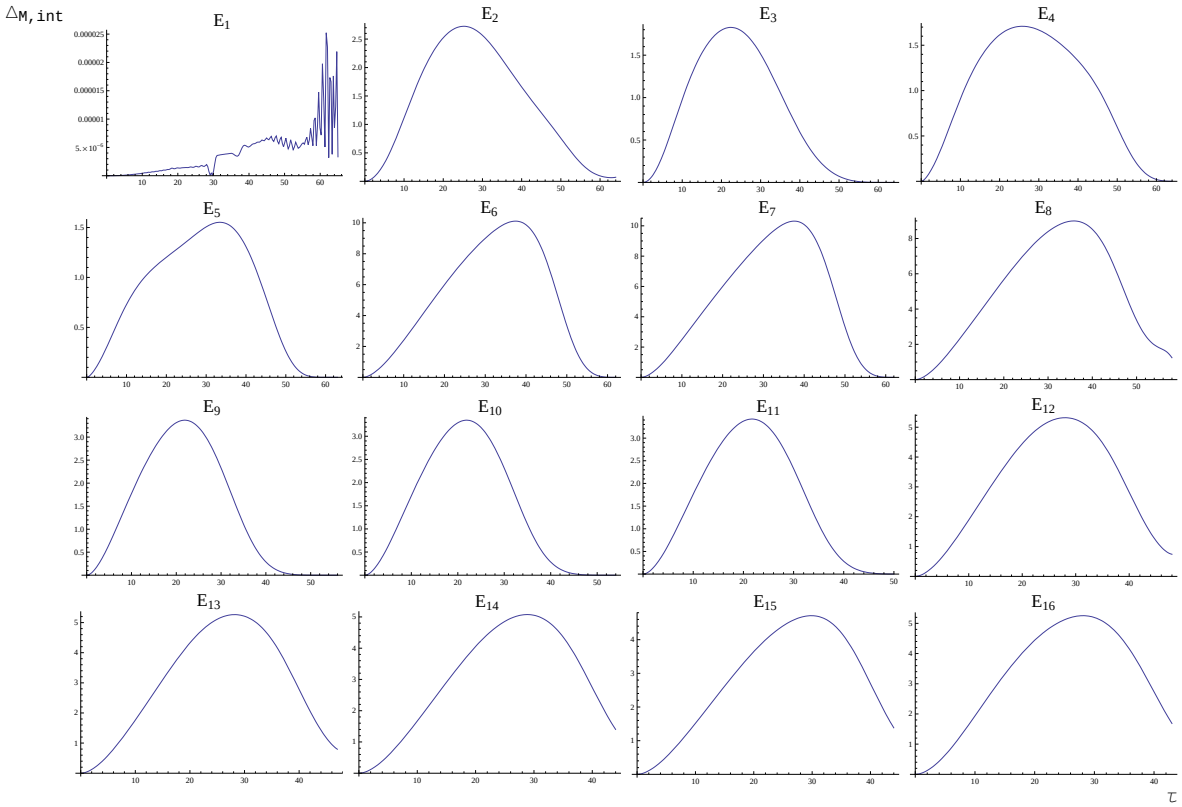

Figure 10: Plots of $\Delta_{M,\mathrm{int}}(\tau)$ for the T-ordered ensembles E_M with $M = 1, \cdots, 16$. We have employed the ansatz for the 'action' $S_M = \frac{L(\tau)^2}{A(\tau)}\left(1 + \frac{c_M(\tau)}{A(\tau)}\right)$.

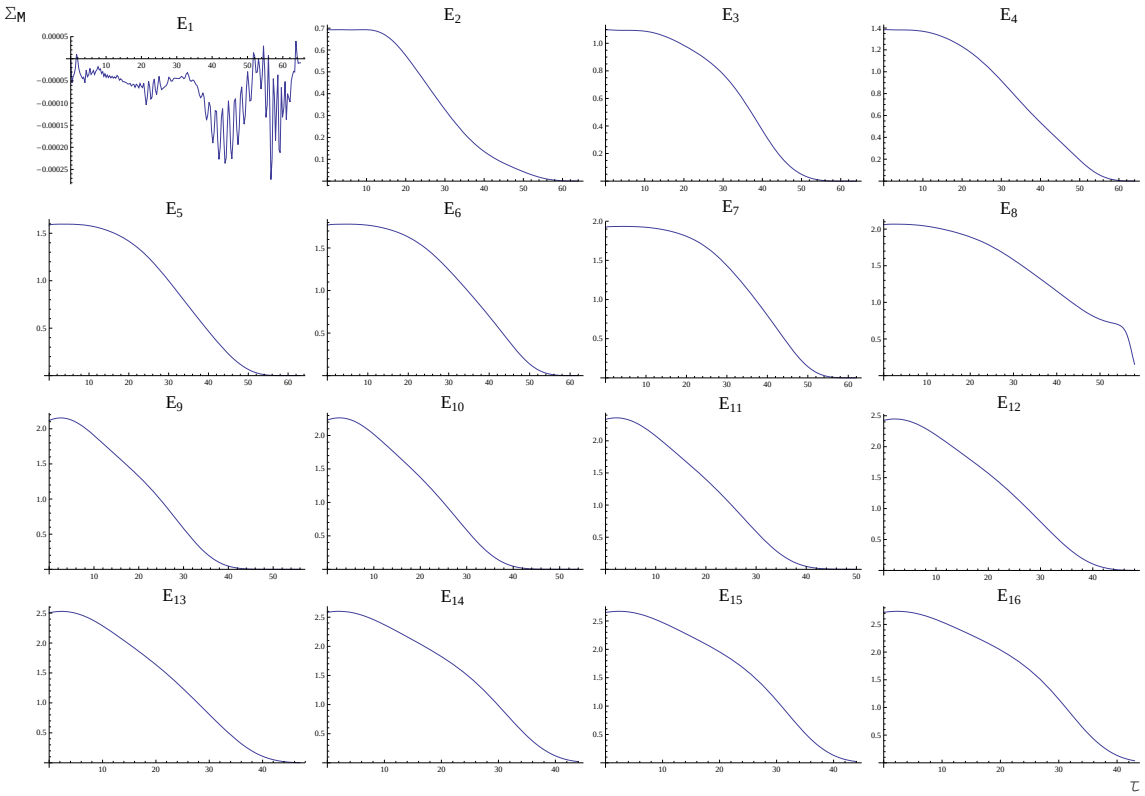

Figure 11: Flow of the entropies Σ_M for T-ordered ensembles of size $M = 1, \cdots, 16$ when evaluated with the 'action' $S_M = \frac{L(\tau)^2}{A(\tau)}\left(1 + \frac{c_M(\tau)}{L(\tau)}\right)$. The situation does not change qualitatively if the 'action' $S_M = \frac{L(\tau)^2}{A(\tau)}\left(1 + \frac{c_M(\tau)}{A(\tau)}\right)$ is used.

3.4 Evolution of entropy

Let us now evaluate the flow of entropy Σ_M defined as

$$\Sigma_M(\tau) \equiv \log Z_M + \frac{1}{Z_M}\sum_{i=1}^{M} \exp(-S_M[\hat{x}_i(\tau)])\, S_M[\hat{x}_i(\tau)] \tag{17}$$

where $S_M[\hat{x}_i(\tau)]$ is given by Eq. (6). In Fig. 11 plots are shown for $\Sigma_M(\tau)$ ($M = 1, \cdots, 16$ when evaluated with the 'action' $S_M = \frac{L(\tau)^2}{A(\tau)}\left(1 + \frac{c_M(\tau)}{L(\tau)}\right)$ for T-ordered ensembles of size $M = 1, \cdots, 16$. These graphs look very much alike to the ones generated using the 'action' $S_M = \frac{L(\tau)^2}{A(\tau)}\left(1 + \frac{c_M(\tau)}{A(\tau)}\right)$. Notice the continuous approach to zero at finite values of τ. This implies that order emerges spontaneously in the system with decreasing resolution: Starting at a finite value of τ, a particular member of E_M is singled out by its weight approaching unity. Judging from our results for the $N = 0$ sector [7], this behavior is highly unexpected. Therefore the nontrivial topology of $N = 1$ induces qualitative differences into the coarse-graining process.

4 Summary, interpretation of results and, conclusion

In this article we have investigated the spatial coarse-graining of CVLs, immersed in a flat 2D plane, of an SU(2) Yang-Mills theory being in its confining phase. The focus was on the sector with one topologically stabilized selfintersection (existence of an isolated magnetic charge at its location, $N = 1$). We have analysed this coarse-graining process in terms of curve ensembles generated by evolving an initial situation under the curve-shrinking flow [8, 9, 12]. The idea here is to suppose that curve shrinking in the parameter τ represents an exact coarse-graining of a given initial state and to re-construct the associated ensemble-weight of the statistical approach (exponential of effective 'action') by demanding invariance of the corresponding partition function under the flow in τ (renormalization-group evolution). Notice that τ is related to a physical resolution, applied to probing the system, in a strictly monotonic decreasing manner. This resolution may be associated with a local momentum transfer exerted by an observer or a globally defined temperature inherent to an environment. The functional dependence of τ on these physical parameters depends on the given experimental situation. It is, however, reasonable to assume that *finite* values of τ universally correspond to *finite* values of these physical parameters.

In Secs. 3.3, 3.4 we have obtained the unexpected result that a statistical ensemble of renormalization-group evolved curves spontaneously orders itself in the sense that, starting from finite values of τ, only a particular member of the ensemble survives the process of 2D spatial coarse-graining. That is, the entropy attributed to the ensemble is practically zero for sufficiently large values of τ. For the location of selfintersection (charge of an electron) this means that no dissipation of energy, provided by the environment, can be mediated by the monopole situated within the core of the intersection if the resolution falls below a critical, *finite* value. This result must drastically depend on the two-dimensionality of space and the fact that we consider the sector with $N = 1$, compare with [7].

The recently discovered, unconventional $FeAs$ systems do not appear to exhibit an explicit, strong correlation between the electrons contained in their theoretically suggested, 2D-superconducting layers, see [13] and references therein. If the two-dimensional behavior of noninteracting electrons, subject to an environment represented by the parameter τ, indeed is described by the coarse-graining process investigated in the present work then the sudden decrease of entropy that we observe at a *finite* value of τ should ultimately be connected to this particular kind of high-T_c superconductivity. Here τ is a monotonically decreasing function of temperature.

Acknowledgments

We would like to thank Francesco Giacosa and Markus Schwarz for useful conversations.

References

[1] W. T. Kelvin and P. G. Tait, *Treatise on Natural Philosophy*, 2 vols., Cambridge University Press, 1867.

[2] J. G. Bednorz and K. A. Müller, Z. Phys. B**64**, 189 (1986).

[3] P. W. Anderson, arXiv:cond-mat/0510053v2.
P. W. Anderson, Physica C**460-462**, 3 (2007).

[4] F. Giacosa, R. Hofmann, and M. Schwarz, Mod. Phys. Lett. A**21**, 2709 (2006).

[5] L. Faddeev and A. J. Niemi, Nature **387**, 58 (1997).
L. Faddeev and A. J. Niemi, Phys. Rev. Lett. **82**, 1624 (1999).
L. Faddeev and A. J. Niemi, Phys. Lett. B **525**, 195 (2002).
L. Faddeev and A. J. Niemi, Nucl. Phys. B **776**, 38 (2007).

[6] R. Hofmann, Int. J. Mod. Phys. A**20**, 4123 (2005); Erratum-ibid.A**21**, 6515 (2006).

[7] J. Moosmann and R. Hofmann, hep-th/0804.3527

[8] M. Gage and R. S. Hamilton, J. Differential Geometry **23**, 69 (1986).

[9] M. A. Grayson, J. Differential Geometry **26**, 285 (1987).

[10] R. Hofmann, arXiv:0710.0962 [hep-th].

[11] F. Giacosa, R. Hofmann, M. Schwarz, Mod. Phys. Lett. A**21**, 2709 (2006).
R. Hofmann, Mod. Phys. Lett. A**22** 2657 (2007).

[12] M. A. Grayson, Invent. math. **96**, 177 (1989).

[13] H.-H. Klauss and B. Büchner, Physik Journal **7**, 18 (2008).